Journal of Catalysis **189,** 91–104 (2000)
Article ID jcat.1999.2687, available online at http://www.idealibrary.com on IDEAL®

Alumina-Supported Copper Chloride

1. Characterization of Freshly Prepared Catalyst

G. Leofanti,*,[1] M. Padovan,*,[2] M. Garilli,* D. Carmello,* A. Zecchina,† G. Spoto,† S. Bordiga,† G. Turnes Palomino,† and C. Lamberti†,[3],‡

*Inovyl Technological Centre, European Vinyls Corporation Italia, Via della Chimica 5, 30175 Porto Marghera, Venezia, Italy; †Dipartimento di Chimica Inorganica, Chimica Fisica e Chimica dei Materiali, Università di Torino, Via P. Giuria 7, 10125 Torino, Italy; and ‡INFM Serione di Torino

Received June 4, 1999; revised September 1, 1999; accepted September 3, 1993

Alumina-supported $CuCl_2$, the basic catalyst for ethylene oxychlorination, has been investigated 1 hour after preparation by UV–vis spectroscopy, a solubility test, EPR, EXAFS, and XRD in a wide range (0.25–9.0 wt%) of Cu concentration. We have evidenced that, at low Cu content, the formation of a surface aluminate species takes place, where isolated Cu(II) ions occupy octahedral vacancies of the alumina surface, having (within experimental errors) five oxygen ligands at 1.92 ± 0.02 Å. The chlorine released by copper chloride during its interaction with alumina gives >Al–Cl species. The formation of this surface copper aluminate stops at 0.95 wt% Cu/100 m^2; at higher Cu concentrations excess copper chloride precipitates directly from solution during the drying step, forming an amorphous $CuCl_2 \cdot 2H_2O$ phase, overlapping progressively the surface aluminate. A slow hydrolysis, giving traces of paratacamite, an insoluble Cu hydroxochloride, also occurs. A room temperature dehydration process up to 10^{-3} Torr implies the evolution of $CuCl_2 \cdot 2H_2O$ into anhydrous $CuCl_2$ as a consequence of the loss of the crystallization water.

Key Words: **Al_2O_3-supported $CuCl_2$; ethylene oxychlorination; copper aluminate; EPR.**

1. INTRODUCTION

Nowadays, almost all the world production of vinyl chloride is based on the cracking of 1,2-dichloroethane, which in turn is produced by catalytic oxychlorination of ethylene with hydrochloric acid and oxygen (1) following this reaction path:

$$C_2H_4 + 2HCl + \frac{1}{2}O_2 \rightarrow C_2H_4Cl_2 + H_2O. \qquad [1]$$

The reaction is performed at 490–530 K and 5–6 atm (1 atm ≈ 1.01 10^5 Pa) using both air and oxygen in fluid- or fixed-bed reactors (2). Commercial catalysts are produced by the impregnation of alumina with $CuCl_2 \cdot 2H_2O$ (4–8 wt% Cu). Other chlorides (mainly alkaline or alkaline earth chlorides) in a variable concentration (1, 3) are added to improve the catalytic performances, making the catalyst more suitable for use in industrial reactors (1, 3, 4).

Despite the great number of investigations since 1973 (5–21), the problem of identifying the structure of all the copper species present on the catalyst is not fully resolved, even in the case of the base catalyst (5–20), i.e., alumina-supported $CuCl_2$ without promoters (the presence of promoters has been studied in Refs. 4, 10, and 21). However, from the published studies, the existence, on base catalyst, of two different Cu compounds or, more exactly, of two different families of Cu compounds is clearly emerging. It has been hypothesized that the first family, prevailing at low Cu concentrations, could result from the interaction between $CuCl_2$ and the Al_2O_3 carrier, while the second family, prevailing at high Cu concentrations, could be the product of the surface precipitation of Cu compounds from the impregnating solution. This picture was suggested mainly by EPR data (5–10), impregnation studies (7, 16, 17), Cu solubility tests (5, 6, 9, 11–15), and TPR measurements (7, 8, 15–18).

EPR studies (5–10) have reported about the presence of two signals exhibiting axial ($g_{xx} = g_{yy} \equiv g_\perp$ and $g_{zz} \equiv g_\parallel$) and spherical ($g_{xx} = g_{yy} = g_{zz} \equiv g_{iso}$) symmetries, sometimes labeled in the quoted papers as asymmetric and symmetric signals, respectively. The axially symmetrical signal prevails (or is the only one present) at low Cu concentrations and is generally attributed, following Baiker *et al.* (7), to highly dispersed or isolated Cu(II) species interacting with the support. The signal reflecting spherical symmetry around Cu(II) ions, which overlaps the first one at high Cu concentrations, is generally attributed to copper chloride clusters or microcrystals of undefined stoichiometry and morphology not interacting with the support (5, 7). Unfortunately, the EPR signal is strongly broadened by spin–spin

[1] Present address: Via Firenze 43,20010 Canegrate, Milano, Italy.
[2] Present address: Via Villa Mirabello 1,20125 Milano, Italy.
[3] To whom correspondence should be addressed. E-mail: Lamberti@ch.unito.it (internet). Fax: +39-011-6707855.

0021-9517/00 $35.00

relaxation processes: as a consequence the local environment around Cu(II) ions cannot be modeled. Moreover, the fraction of Cu(II) ions contributing to the EPR signal is unknown but likely low, particularly when aggregated species are present.

Solubility tests in water or acetone (5, 6, 9, 11–15) have pointed out that the copper species becomes partially insoluble after interaction with the support, so indicating that a fraction of Cu has been transformed from $CuCl_2$ (an easily soluble Cu compound) into one or more insoluble compounds.

As far as TPR measurements are concerned, we stress the fact that the attempt made in the past to associate the two peaks observed in TPR profiles to two Cu(II) species (7, 8, 16, 17) must be discarded in the light of more recent results (15, 18), which demonstrate that the two peaks correspond to a two-step $Cu(II) \rightarrow Cu(I) \rightarrow Cu(0)$ reduction. This result likely indicates that the reduction temperatures of the two families of Cu(II) species mentioned before (and subsequent Cu(I) species) are too close to be resolved by TPR. In other words, TPR is not diagnostic of the different structures.

Even if most authors have reached a substantial agreement about the presence of two different families of Cu(II) compounds on alumina-supported $CuCl_2$, the nature of such compounds is still under debate. In the two following paragraphs the different hypotheses presented in the literature concerning the predominating species on samples with low and high Cu content will be briefly summarized.

As far as low concentrated samples are concerned, Baiker and co-workers (7, 16, 17) attributed the axially symmetric EPR signal to a highly dispersed or isolated Cu(II) species similar to those found on Cu–Y or on Cu-doped $MgAl_2O_4$. It has been hypothesized that this species has a tetragonally distorted octahedral configuration with oxygen in the first coordination sphere. Blanco *et al.* (5, 6) have compared EPR, solubility test, and XRD results on a set of samples with Cu content in the 0.8–10.5 wt% Cu range. They report that soluble copper species can be detected starting only from 4.6 wt% Cu and can increase with increasing copper loading. They conclude that the species prevailing at low Cu concentrations is $Cu_x(OH)_yCl_2$, while that dominating for higher copper content is paratacamite $Cu_2(OH)_3Cl$ (as evidenced by XRD results starting from the 2.5 wt% sample). On the basis of EPR solubility tests and DTA results, Resasco *et al.* (9, 10, 13) showed that at low Cu concentrations (1 wt%) the axially symmetric EPR signal does not change either after extraction with acetone or after heating at 633 K. Notice that while in their earlier work (13) they agreed with Blanco *et al.*'s conclusions (6), in a more recent one (10) they suggest that the interaction with Al_2O_3 gives a very stable Cu–O–Cl surface species. A few other authors, in papers devoted to parallel aspects of the topic, such as the effect of different carriers or additives, have discussed briefly the nature of Cu-interacting species in a $CuCl_2/Al_2O_3$ system. Here, we quote (i) the $(=Al_2O)_2 \rightarrow CuCl_2$ species hypothesized in the first paper of Blanco *et al.* (5) and tentatively proposed by Arcoya (19) afterwards, (ii) a monodispersed positive oxidation state of Cu suggested by Sermon (8), (iii) the monolayer of interacting species proposed by Sai Prasad *et al.* (14), (iv) atomically dispersed species interacting via oxygen bonds with the support as reported by Bond *et al.* (18), and (v) an attached bidimensional phase strongly interacting with the support (15). From this brief overview it is evident that the exact nature of the copper species, in low Cu concentrated samples, is still not assessed and that most authors are in favor of a highly or atomically dispersed Cu(II) compound interacting with alumina and probably containing both oxygen and chlorine in its coordination sphere.

As far as the species in samples with high Cu content are concerned, two main Cu compounds have been identified: $CuCl_2$ and $Cu_2(OH)_3Cl$ (paratacamite). Taking into account that $CuCl_2$ is the only soluble Cu compound among those containing Cl and O, solubility tests with water or acetone should allow its direct and quantitative detection. However, when a quantitative comparison of the soluble fractions reported in the different papers (5, 6, 9, 11–15) is made, very consistent discrepancies are found. This is probably due to different preparation and thermal treatment procedures. With the only exception of Ref. (5), the picture emerging from literature suggests the presence, at high Cu concentrations, of soluble $CuCl_2$, which is not detectable by XRD, owing to its high dispersion on the large support surface. Paratacamite, on the contrary, is predominant in the XRD patterns of samples with a Cu concentration of 2.5 wt% or higher. It has been suggested that its formation is due to slow hydrolysis of $CuCl_2$ catalyzed by basic sites of the alumina surface (12). Finally, in the contributions of Solomonik *et al.* (20), on the basis of XRD results, it is suggested that, besides $CuCl_2$ and paratacamite, CuO, $CuAl_2O_4$, and $CuAlO_2$ are also present. However, we believe that only the presence of paratacamite can be safely inferred from the inspection of reported XRD patterns (see, e.g., Fig. 2 of Ref. (20b)].

In conclusion, it is evident that the nature of different compounds, present on alumina-supported $CuCl_2$ catalysts, is far from being satisfactorily understood. This is particularly true for the species present on samples with low Cu content. As far as higher concentrations are concerned, the relation among different species (relative abundance ratio) and the possibility of reciprocal transformation upon aging and thermal treatments are not sufficiently clear. As a matter of fact, the possible presence of changes with time has been suggested only in Ref. (12) on the basis of reflectance NIR data. In our contribution it will be shown that aging time is an additional parameter which must be considered and which can explain most of the relevant

discrepancies found in the literature data when a quantitative comparison of the soluble fractions of copper is made. Finally, let us remark that no information is available on the evolution of the hypothesized copper species when the temperature is increased up to the values typical of oxychlorination reaction. Consequently, the aim of our study is threefold: (i) identification of the species present at different Cu content, (ii) determination of their concentration, and (iii) study of the transformations induced by aging and thermal treatments. The study has been performed on a set of samples covering a wide range of copper loading (0.25–9.0 wt%) and treated in different conditions: on the fresh catalyst (i.e., immediately after impregnation of alumina), after aging for 24 h and 6 months at room temperature and after heating up to the values typical of oxychlorination reaction (500–550 K). To fulfill this task, we have used different complementary techniques such as XRD, UV–vis-NIR DRS, IR, EPR XAES, EXAFS, a solubility test, and an activity test in ethylene oxychlorination. In particular, in the present paper we report the results obtained on the fresh catalysts only, while in a subsequent one (22) the effect of aging and thermal treatments will be discussed.

2. EXPERIMENTAL

2.1. Materials

Six $CuCl_2$/alumina samples (having a Cu content of 0.25, 0.5, 1.4, 2.3, 4.6, and 9.0 wt%, respectively) were prepared by impregnation of γ-alumina (Condea Puralox SCCa 30/170: surface area, 168 $m^2\ g^{-1}$; pore volume, 0.50 $cm^3\ g^{-1}$) with an aqueous solution of $CuCl_2 \cdot 2H_2O$ following the incipient wetness method. A highly diluted sample (0.035 Cu wt%) has been prepared *ad hoc* for EPR measurements only, with the aim to eliminate the undesired spin–spin relaxation phenomena among Cu(II) ions always present in more concentrated samples. After impregnation, the samples were dried at room temperature (RT) under a dry air flow for 1 h and then kept at RT. The characterization of the samples has been performed 1 h after impregnation. To clarify some peculiar aspects of the argument under study, the characterization of few samples treated in different conditions has been performed (as detailed in the text). The copper content is used to identify the samples: for example, Cu2.3 indicates the sample containing 2.3 wt% Cu.

For the sake of comparison the same measurements with physical techniques have been performed also on a few model compounds: $CuCl_2 \cdot 2H_2O$, CuO, Cu_2O, CuCl, $CuCl_2$, $Cu_2(OH)_3Cl$, and CuO0.25. $CuCl_2 \cdot 2H_2O$, CuO, Cu_2O, and CuCl commercial products have been used. $CuCl_2$ was obtained by drying $CuCl_2 \cdot 2H_2O$ at 423 K, while $Cu_2(OH)_3Cl$ was prepared by boiling 1 g of CuO (Carlo Erba) in 500 cm^3 of an aqueous solution containing 150 g of $CuCl_2 \cdot 2H_2O$ (Carlo Erba). After 5 h the slurry was filtered, washed, and dried at 333 K. The identity of the obtained compound was checked by XRD. Sample CuO0.25 was prepared by impregnation of γ-alumina Condea Puralox SCCa 30/170 with an aqueous solution of $Cu(NO_3)_2 \cdot 2H_2O$ following the incipient wetness method. After impregnation the samples were dried at 310 K under air flow for 1 h and then calcined at 673 K to decompose the nitrate. Analogous with the convention already adopted for samples prepared from $CuCl_2$, the number 0.25 indicates the wt% of the copper concentration.

2.2. Methods

The copper content was determined by mixing 300 mg of sample with 5 cm^3 of demineralized water and 5 cm^3 of HNO_3 37% solution. After 10 min of heating at the boiling point, the solution was cooled down to RT and filtered to separate the solid alumina residue. AAS measurements with a Perkin Elmer 3030 spectrophotometer were then performed on the so-obtained clear solution opportunely diluted. The chlorine content was determined by treating 300 mg of dried sample with 5 cm^3 of HNO_3 37% solution. The mixture was then stirred for 30 min at RT, filtered, and diluted. A potentiometric titration was then carried out on the solution by using a standard solution of $AgNO_3$, 0.05 N.

A Perkin-Elmer Lambda 15 spectrophotometer, equipped with an integrating sphere, was used to perform the UV–vis DRS measurements in the range 12,500–50,000 cm^{-1}. In a few cases the measurement range was extended to 7500 cm^{-1} by using a Perkin-Elmer Lambda 9 spectrophotometer.

The XRD patterns were collected at RT by a Siemens D500 θ/θ diffractometer using Ni-filtered Cu$K\alpha$ radiation at 40 kV and 30 mA. Diffraction intensities were collected in the 5°–90° 2θ range.

EPR spectra have been measured at liquid nitrogen temperature on a Varian E 109 spectrometer equipped with a dual cavity and operating in the X band. Varian Pitch was used as a reference for the calibration of g values. Before cooling, samples were evacuated at RT up to 10^{-3} Torr (1 Torr = 133.3 Pa).

Solubility tests were performed by stirring 100 mg of sample in 50 cm^3 of ethyl alcohol at RT because it easily dissolves $CuCl_2$, but neither basic chlorides (as paratacamite) nor oxychlorides and other oxygenated compounds (23). After 2 h the slurry was filtered and washed with ethyl alcohol and the liquid, after appropriate dilution, was used to measure the copper concentration by UV–vis spectroscopy (after calibration experiments with copper chloride solutions at various concentrations).

X-ray absorption measurements were carried out using synchrotron radiation of the EXAFS1 station at LURE (Orsay, France) during the same experiment where also Cu-ZSM-5 (24 a,b) and Cu-MOR (24c) catalysts were measured. We shall so refer to Ref. (24) for all technical details

concerning data acquisition. A number ranging between three and five (depending on the Cu loading) EXAFS spectra were recorded in the same experimental conditions for each samples. Extracted $\chi(k)$ have been averaged before the EXAFS data analysis. The standard deviation calculated from the averaged spectra was used as an estimate of the statistical noise for the evaluation of the error associated with each structural parameter. Experimental $\chi(k)$ was extracted from absorption data as described in detail in Ref. (24a), with the only exception that in this case a 6th degree polynomial fit was used to estimate the atomic-like contribution. The k^3-weighted $\chi(k)$ were Fourier-transformed over a Kaiser window, with $\tau = 2.5$, in the 2.65- to 13.65-$Å^{-1}$ range. Main contributions to the Fourier transform modulus were filtered to obtain the Cu-nearest neighbor shell. The so-obtained filtered contribution was analyzed using programs developed by Michalowicz (25), following standard procedures (26). The Cu–Cl and Cu–O contributions, in filtered EXAFS spectra, have been modeled using phase shift and amplitude functions extracted from McKale files (27) and from a Cu_2O (4 equiv of oxygen at 1.85 Å (28)) model compound, respectively: CuO exhibiting four different oxygen atoms at 1.91, 1.93, 1.98, and 2.02 Å, respectively (29) could not be considered a good candidate. The transferability of Cu–O phases and amplitudes extracted from a Cu(I) model compound into samples where copper is in the oxidation state of +2 has been tested on the first shell filtered EXAFS spectra of CuO, which was satisfactorily well-reproduced with two subshells at the crystallographic fixed values of $N_1 = 2$, $R_1 = 1.92$ Å and $N_2 = 2$, $R_2 = 2.00$ Å.

3. RESULTS AND DISCUSSION

The most important aim of this paper concerns the elucidation of the composition and of the structure of the freshly prepared alumina-supported $CuCl_2$ catalyst. To achieve this goal, a series of six samples with a Cu concentration ranging from 0.25 to 9.0 wt% has been examined in detail with several physico–chemical techniques. In particular, in the following subsection (3.1) we will discuss the presence of two different families of Cu compounds, as suggested by the literature (*vide supra*: Introduction), and the influence of Cu loading in determining their relative concentrations. Afterward, the nature and the structure of the copper species dominating at low and high Cu concentrations will be discussed in greater detail (subsections 3.2 and 3.3, respectively).

3.1. Existence of Two Families of Cu(II) Species

Let us start first by commenting on the results obtained by means of UV–vis spectroscopy reported in Fig. 1. The spectral range can be divided into two parts: 10,000–22,000 cm^{-1} and 22,000–50,000 cm^{-1}. In the first range, a band with a maximum at about 13,000 cm^{-1}, due to a d–d $^2E_g \rightarrow {}^2T_{2g}$ transition characteristic of Cu(II) ions in octahedral complexes is observed (30). In the second range, a wide and complex absorption with a charge transfer (CT) character is found. This absorption is fully located in the UV part of the spectra for low copper-loaded samples and partially in the visible part too for high Cu-concentrated samples (Fig. 1). Several important considerations can be extracted from the reported spectra. The intensity of the d–d transition increases with Cu content, but the trend is far from being linear, showing a sharp increase between 1.4 and 2.3 wt% Cu. As it is well-known that in homogeneous complexes the intensity of the band is influenced by any deviation from octahedral symmetry, caused by the presence of chemically nonequivalent ligands, this behavior indicates that in the 1.4–2.3 wt% Cu range an abrupt change in the ligands sphere is occurring. It is worth noticing that, on samples with high copper concentration, the intensity of the d–d transitions reaches very high values comparable to those of the CT bands. While samples with Cu concentrations lower than 1.4 wt% show a single CT band with a maximum in the 40,000- to 43,000-cm^{-1} range (samples Cu0.25–Cu1.4), samples with Cu concentrations higher than 2.3 wt% show a new CT band with a maximum in the 28,000- to 31,000-cm^{-1} range, which develops progressively as the copper concentration increases. It is worth underlining that on high Cu-loaded samples both CT bands are present, so suggesting the co-presence of two different Cu(II) species. The comparison of the results concerning the d–d and CT regions suggests that the first shell ligands of Cu(II) species present in the 0.25–1.4 wt% samples and those formed starting from the Cu2.5 sample are different. The species present at low Cu concentrations are characterized by a

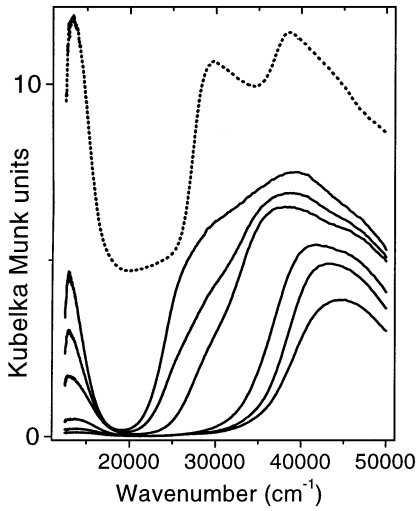

FIG. 1. UV–vis DRS spectra of 1-h aged samples and hydrated $CuCl_2$ model compound. From top to bottom: $CuCl_2 \cdot 2H_2O$ (dotted line curve vertically shifted for graphical reasons), Cu9.0, Cu4.6, Cu2.3, Cu1.4, Cu0.5, and Cu0.25 samples (full line curves).

high-frequency (40,000–43,000 cm^{-1}) CT transition and by a low intensity *d–d* band at about 13,000 cm^{-1}, typical of an octahedral species containing chemically equivalent ligands. The species dominating at high Cu concentrations shows an additional low-frequency (28,000–31,000 cm^{-1}) CT transition and a high-intensity *d–d* band again at about 13,000 cm^{-1}. Similar features characterize the UV–vis spectrum of $CuCl_2 \cdot 2H_2O$ (dotted curve in Fig. 1). While the high intensity of the *d–d* band is indicative of the presence of ligands heterogeneity in the Cu(II) coordination sphere, the constancy of the peak frequency along the sample series suggests that the average ligand field strength is not appreciably changing from low to high Cu concentration.

Further proof of the existence of two kinds of copper species, together with some information on their different behavior upon thermal treatments, arises from the study of the effect of heating. In fact, the UV–vis spectra of low-concentrated samples remain substantially unchanged after heating at 923 K (Fig. 2a for the Cu0.25 sample). The spectra of Cu0.5 and Cu1.4 samples, not reported for the sake of brevity, exhibit the same constant behavior. As 923 K is a temperature high enough to assure a nearly complete removal of chlorine from the solid, we can safely exclude that chlorine anions are present in the coordination sphere of Cu(II) on low-concentrated samples. On the contrary, the UV–vis spectra of high copper-loaded samples show significant changes upon heating, involving both *d–d* and CT transition bands. In particular, the CT band at 28,000–31,000 cm^{-1} (Fig. 2b: Cu9.0 sample) disappears while the intensity of the *d–d* band decreases. Simultaneously, the chlorine content of the Cu9.0 sample decreases dramatically to 0.6 wt% Cl (corresponding to a reduction of the Cl/Cu atomic ratio from 2.0 to 0.1). It is so concluded that the change in the ligand sphere of Cu(II), indirectly observed by UV–vis spectroscopy on high Cu-loaded samples upon heating at 923 K, is associated to a loss of Cl atoms.

The solubility test results reported in Fig. 3, strongly support the above picture. The full line reported in Fig. 3 corresponds to the theoretical solubility of copper (if totally constituted by $CuCl_2$), while triangles represent the experimental values. The points corresponding to non-null solubility values have been interpolated by the dashed line. At each abscissa value, the difference between full and dashed lines represents the contribution of insoluble copper. From Fig. 3 it is evident that, at low copper concentration, only insoluble Cu species are present. Starting from sample Cu2.3 soluble species appear, whose concentration increases linearly with the Cu content. This result agrees well with the appearance of the new CT band in the 28,000- to 31,000-cm^{-1} range and with the marked increase of the *d–d* band intensity observed starting from sample Cu2.3. It is worth noticing that the full and dashed lines are parallel, so implying that the insoluble fraction remains constant in the

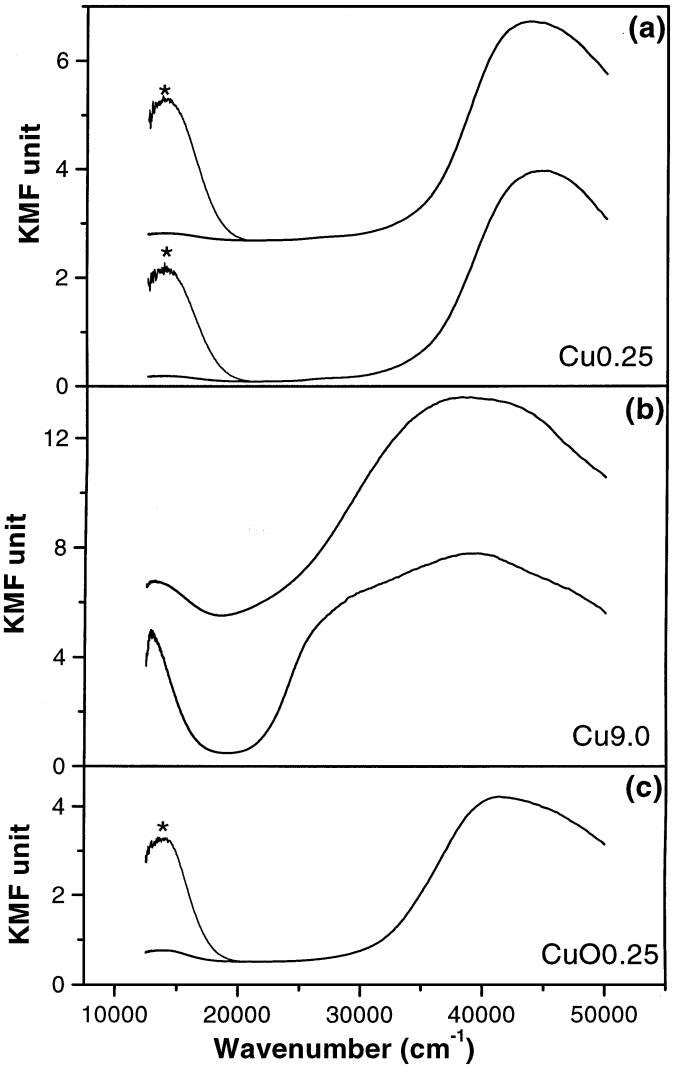

FIG. 2. UV–vis DRS spectra before (lower curve) and after (upper curve) heating at 923 K for samples Cu0.25 and Cu9.0, parts (a) and (b) respectively. Part (c) reports, for comparison with the lower spectrum of part (a), the UV–vis DRS spectrum of sample CuO0.25 heated at 673 K to remove nitrates. All curves have been vertically shifted. In parts (a) and (c) the *d–d* transition band has been magnified by a factor of 20 in the 12,500- to 20,000-cm^{-1} range to allow a detailed comparison (see stars).

2.0–9.0 Cu wt% range. In turn, this means that the soluble species appearing at high Cu loading is not substituting the insoluble Cu species formed at low copper concentrations. This evidence definitively confirms that the two CT transitions belong to different species.

Figure 4a reports the progressive evolution of the EPR signal, collected at liquid nitrogen temperature, as a function of the Cu loading. The spectrum of a highly diluted sample Cu0.035, prepared *ad hoc* for EPR study (*vide infra* section 3.2), has also been included in Fig. 4a. All samples have been evacuated at RT up to 10^{-3} Torr before cooling to eliminate the excess water always present on the

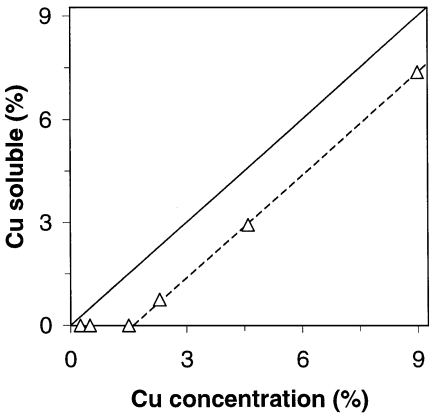

FIG. 3. Dependence of copper solubility on copper concentration, pointing out the effect of copper content on copper species present on the solid. (Δ) experimental points; (broken line) linear interpolation among data with non-null solubility; (full line) line representing a hypothetical 100% solubility. As a consequence, for each experimental point, the difference between the ordinate of the full line and that of the Δ symbol gives the amount of insoluble copper.

as-prepared samples. This treatment has shown to have a null effect on the low Cu-loaded samples, while starting from Cu2.3, high Cu-loaded samples undergo a color change from green to brown. The different stability of low and high Cu-loaded samples upon evacuation reflects what has already been observed upon heating (Figs. 2a and 2b) and is further evidence supporting the presence of two different Cu(II) species. Even from a superficial investigation, it is evident that spectra of low loaded samples are typical of Cu(II) ions in axial symmetry ($g_{xx} = g_{yy} \equiv g_{\perp}$ and $g_{zz} \equiv g_{\parallel}$) (5–10). For samples Cu0.25, Cu0.5, and Cu1.4, the splitting into quartets, due to the hyperfine interaction between the unpaired electron and the copper nucleus (both ^{63}Cu and ^{65}Cu nuclei have a 3/2 nuclear spin (31)), is clearly visible only in the parallel component, while the perpendicular one exhibits only shoulders (samples Cu0.25 and Cu0.5) or is completely unresolved (sample Cu1.4). Moving to high loaded samples, any vestige of the hyperfine structure is progressively lost, being totally absent for Cu9.0. This sample exhibits a broad EPR spectrum with a slope typical of an isotropic g tensor ($g_{xx} = g_{yy} = g_{zz} \equiv g_{iso}$) (5–10). However,

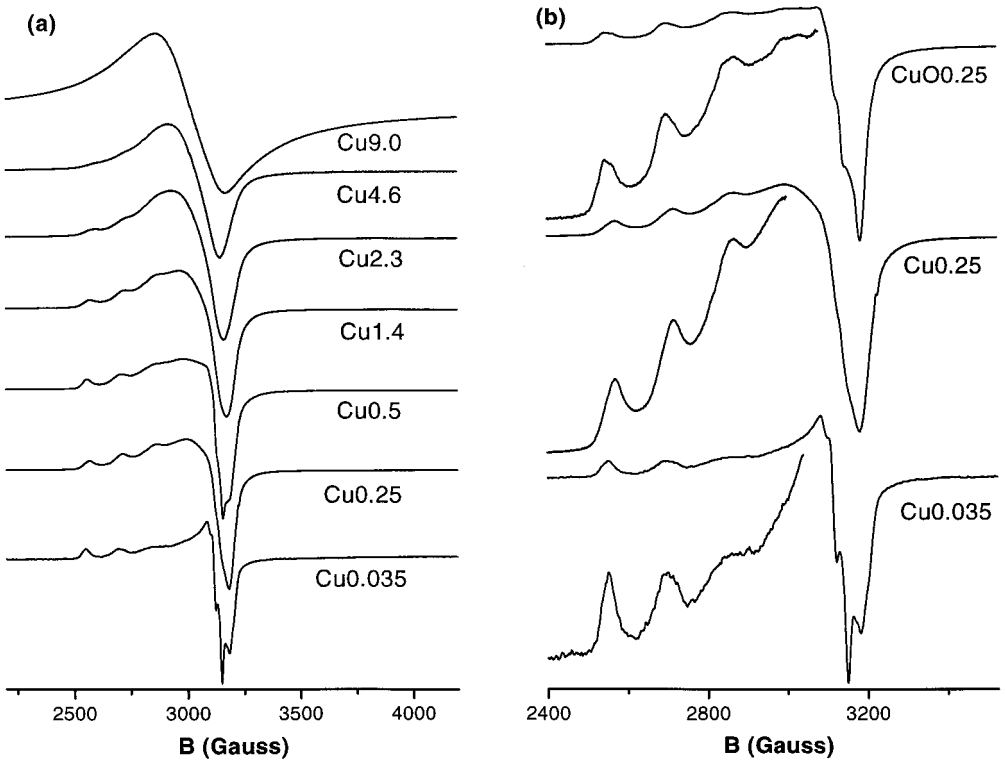

FIG. 4. Part (a): liquid nitrogen temperature EPR spectra of all samples. Cu content increases from bottom to top. The amplitude of the EPR signal of all samples has been multiplied by different factors for graphical reasons. Before cooling, samples were evacuated at RT up to 10^{-3} Torr. The color of low Cu-concentrated samples (up to Cu1.4 included) is not affected by this treatment; on the contrary, the color of high-loaded samples turns from green to brown upon evacuation: this fact has been interpreted by the lost of crystallization water of hydrated $CuCl_2$ (green-colored), giving rise to anhydrous $CuCl_2$ (brown-colored), *vide infra* section 3.3. All EPR spectra reported here reflect the magnetic environment of Cu(II) species in dehydrated samples. Part (b): zoom in the 2400- to 3525-G range for samples Cu0.035 (bottom spectrum) and Cu0.25 (middle spectrum). For comparison, the spectrum of sample CuO0.25 (prepared from nitrate) is also reported (top spectrum). In the 2400- to 3000-G interval, below each spectrum, the corresponding magnificated $g_{\parallel}$ signals is reported.

when the sequence of spectra reported in Fig. 4a is analyzed, the hypothesis of the contribution of an axial signal to the spectrum of sample Cu9.0 cannot *a priori* be excluded. In fact, a relevant asymmetry is still present in the spectrum of sample Cu4.6. In our opinion, a firm conclusion about this point will be drafted only after a systematic simulation of the whole set of spectra, which is in progress and will be presented in a successive paper, is made. We can so conclude that, in agreement with the EPR data reported in the literature (5–10), we have observed (upon increasing the copper loading) the progressive overshadowing of the axial signal observed on low Cu-concentrated samples by a broad EPR signal attributed to a different family of Cu(II) species probing either a symmetrical magnetic environment or a strongly broadened one, again with axial symmetry.

3.2. The Structure of Copper Species on Low Cu-Concentrated Samples

Before discerning about the structure of Cu species, we will briefly summarize the properties of the Cu species predominating at the lower copper-loaded samples as inferred from the above-reported results: (i) the species are insoluble; (ii) their concentration on alumina reaches a maximum at about 2 wt% Cu and then remains constant at higher Cu concentration; (iii) they are characterized by a low intensity *d–d* band at about 13,000 cm^{-1} and by a single CT band in the 40,000- to 43,000-cm^{-1} region; (iv) the species are not affected by a dehydration treatment at RT nor by a heating treatment at a temperature sufficient to remove nearly all the chlorine present in the sample; (v) they give rise to an axially symmetric EPR signal.

The absence of chlorine from the first coordination sphere of copper and the stability under heating allow the comparison with samples prepared with a chlorine-free–copper source. Samples with low copper concentration prepared by impregnation of alumina with copper nitrate and calcined at about 600–700 K satisfy these requirements. These samples have been widely investigated (32–43) and their knowledge can be used as a guideline for interpreting our results. When this route has been followed, sample CuO0.25 has been prepared.

Let us begin from the fact that Cu0.25, Cu0.5, and Cu1.5 samples are characterized by EPR spectra, reflecting an axial symmetry (see Fig. 4a) with value for $g_\parallel$ and $g_\perp$ close to those reported in the literature for the $CuCl_2/Al_2O_3$ system (low Cu loading), or for other chlorine-free–copper compounds (5, 6, 32–36). However, the samples prepared via $CuCl_2$ exhibit a less resolved hyperfine structure when compared with those obtained from nitrate with comparable Cu concentration (see Fig. 4b where the spectra of Cu0.25 and CuO0.25 samples are reported (top curves)). The perpendicular hyperfine lines are definitively better resolved for CuO0.25 than for the Cu0.25 sample. To minimize the spin–spin interaction effect and to obtain EPR spectra of magnetically isolated (or nearly isolated) Cu(II) ions, we have *ad hoc* prepared a highly diluted sample (Cu0.035, bottom spectrum in Fig. 4b). As desired, its EPR spectrum is typical of a nearly isolated Cu(II) species: the axial symmetry of the signal suggests the location of Cu(II) in surface octahedral vacancies of alumina. A preliminary modeling of the experimental signal suggests the presence of at least two slightly different Cu(II) sites, together with a weak broadening effect due to a spin–spin interaction present, even in a so-diluted sample. However, the interference between neighboring Cu(II) centers can be in a first approximation neglected and the main contribution to the spectrum can be described in terms of an axial spectrum whose spin-Hamiltonian parameters (averaged over the two sites) are $g_\parallel = 2.32$, $g_\perp = 2.06$, $A_\parallel = 150$ G and $A_\perp = 12$ G, values very close to those observed on samples obtained from nitrates (see, e.g., Refs. 33 and 44). To the best of our knowledge, the EPR spectrum of Cu0.035 is the first one exhibiting such a resolution among those obtained on $CuCl_2/Al_2O_3$ samples. A detailed simulation of this spectrum is in progress; however, for the purposes persecuted in this work, the qualitative information so far obtained from EPR spectroscopy is of great relevance in confirming similarities between the Cu(II) environment in samples obtained from nitrate and in low loaded-$CuCl_2/Al_2O_3$ samples. The presence of at least two families of sites having a slightly different magnetic environment (both with axial symmetry) is not surprising due to the rather defective character of the γ-Al_2O_3 surface. Note that these two EPR signals can also be tentatively ascribed to Cu(II) occupying surface octahedral sites of two crystallographic different γ-Al_2O_3 faces.

This similarity is further confirmed by UV–vis spectroscopy, as shown in Fig. 2, where the spectra of Cu0.25 and CuO0.25 samples are compared (lower curve in part (a) and curve in part (c) respectively). Notice that similar spectra can be found in the literature on samples prepared from nitrate (36–43): in fact, in all the cases the *d–d* transition (weak) is in the 12,500- to 13,500-cm^{-1} range and a single CT band appears in the 40,000- to 43,000-cm^{-1} range. The *d–d* transition at about 13,000 cm^{-1} has been assigned to copper ions in an octahedral configuration in surface compounds (32, 33, 36–42). In particular, cited authors conclude that copper ions enter the surface octahedral interstices of the spinel structure of γ-Al_2O_3, assuming a typical tetragonally distorted octahedral configuration. The absence of detectable bands of electronic origin below 10,000 cm^{-1} (Fig. 5) confirms that the fraction of copper ions entering the tetrahedral vacancies of the alumina surface is negligible (32, 33, 38–42): this is different from what is expected for the bulk spinel, where about 60% of copper ions is in a tetrahedral coordination (43). This conclusion is based on the fact that the presence of copper in tetrahedral coordination should be easily detected by NIR spectroscopy because the involved *d–d* transition ($^2T_2 \rightarrow {}^2E$) is expected at about

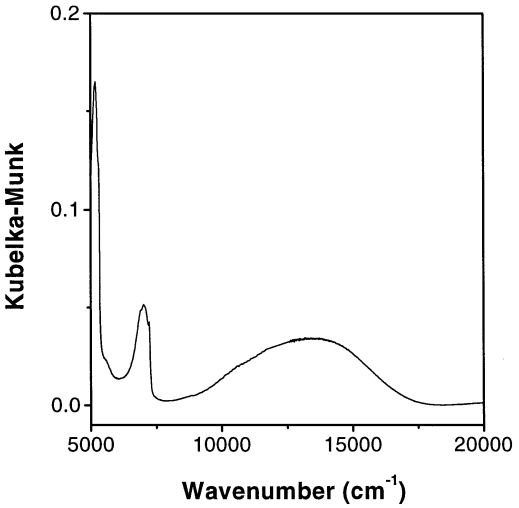

FIG. 5. Vis–NIR spectrum of the Cu1.4 sample.

7,000 cm^{-1} and should have an extinction coefficient at least 1 order of magnitude larger than that of octahedral Cu(II) (33, 38, 41). The weak and narrow bands observed in the 5,000- to 10,000-cm^{-1} region (Fig. 5) have a vibrational origin and are attributed to overtones and to a combination of [OH] group vibrations of water molecules adsorbed on the surface (band at about 7,000 $cm^{-1} = 2\nu$(O–H) and strong and narrow band at 5225 $cm^{-1} = \nu$(O–H) + δ(H–O–H)).

In conclusion, the spectroscopic evidence confirms that Cu(II) is in octahedral coordination. Moreover, from the comparison with the EPR and UV–vis spectra of calcined $Cu(NO_3)_2/Al_2O_3$ samples, we can hypothesize that Cu(II) forms surface aluminate species with oxygen atoms in the first coordination sphere.

Direct evidence of the formation of surface aluminate species can come from EXAFS results. In fact, the atomic selectivity of this technique makes EXAFS a powerful tool in the characterization of active centers (45), because it gives information on the coordination numbers, distances, and chemical nature of the atoms forming the first coordination spheres of Cu(II).

EXAFS measurements have been performed at LURE Laboratories (see the Experimental) on 6-month aged samples and not on the freshly prepared catalysts. Notwithstanding this fact, EXAFS results can be used to characterize low Cu-content samples (up to Cu1.4) since we have demonstrated that aging does not have consequences on the low-concentration samples (22). EXAFS data on more concentrated samples (Cu2.3 and Cu9.0) will be discussed in the next paper, where the effect of aging will be systematically reported (22). The upper curve in Fig. 6a represents the background-subtracted k-weighted $\chi(k)$ EXAFS function of the Cu1.4 sample *in vacuo* at RT. The absence of any beat in this function suggests that the main contribution to the overall signal comes only from the first coordination shell of the copper absorbers. The k^3-weighted, phase-uncorrected, Fourier transform (FT) function, calculated over the range 2.65–13.65 $Å^{-1}$ ($\Delta k = 11.0$ $Å^{-1}$), gives only one peak at 1.53 Å, as shown in the full line curve of Fig. 6b. Insignificant contribution emerges from the second shell environment, implying a considerable static disorder or heterogeneity of second shell neighbors around copper. The first shell contribution was then filtered in the 0.85- to 2.00-$Å^{-1}$ range ($\Delta r = 1.15$ Å: $2\Delta k \Delta r/\pi = 8$) and modeled as Cu ions coordinated to N oxygen atoms. The Cu–O phase and oxygen-scattering amplitude have been extracted from the Cu_2O reference spectrum. The quality of the fit can be appreciated in the middle curves reported in Fig. 6a (dotted and full lines for experimental and fit, respectively). The numerical values thus obtained for the coordination number of Cu(II) ions (N)

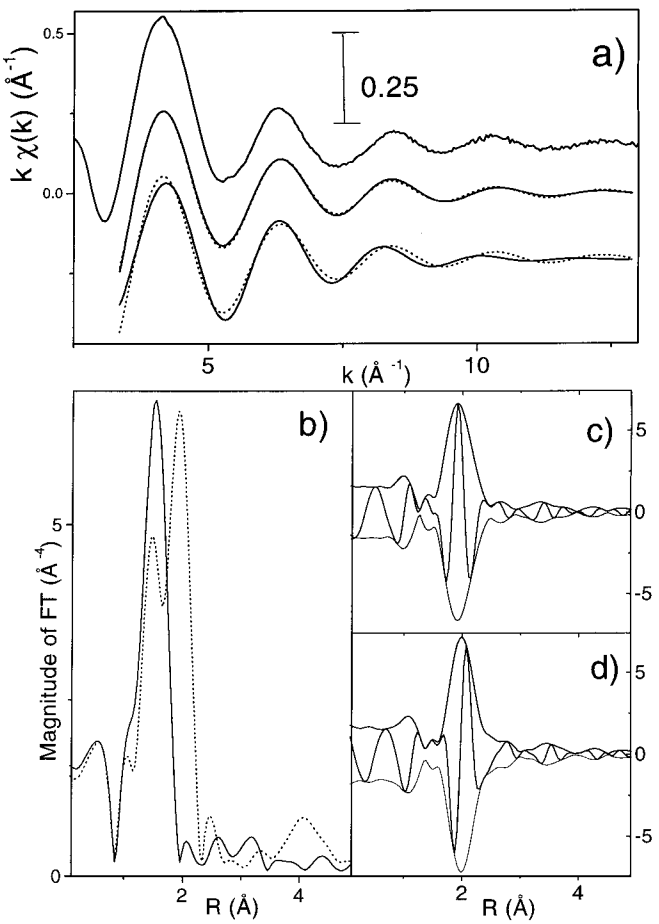

FIG. 6. EXAFS study on sample Cu1.4. Part (a): raw EXAFS data (upper curve), first shell filtered $\chi(k)$ and comparison with best fit obtained using Cu–O (middle curves) and Cu–Cl (lower curves) models, respectively. Part (b): k^3-weighted, phase-uncorrected, FT for the Cu1.4 sample and $CuCl_2 \cdot 2H_2O$ model compound, full and dotted lines, respectively. Part (c): modulus and imaginary part of the k^3-weighted and Cu–O phase-corrected, FT for the Cu1.4 sample. Part (d) as part (c) using the Cu–Cl phase for the correction.

and Cu–O bond lengths were as follows; $N = 4.8(\pm 0.5)$ and $r(\text{Cu–O}) = 1.92(\pm 0.02)$ Å, using $\Delta E = -8.3(\pm 2.0)$ eV. The relative Debye–Waller factor resulted in $\sigma = (8.9 \pm 1.0)10^{-2}$ Å, taking arbitrarily $\sigma = 6.8 \times 10^{-2}$ Å for Cu_2O. The comparison between σ values indicates a slightly higher thermal (or static) disorder of our sample with respect to Cu_2O. The copper precursor being $CuCl_2$, the same first shell filtered spectrum has also been modeled as Cu–Cl contributions. The best fit of this analysis is reported in the bottom spectra of Fig. 6a (full line) together with the experimental signal (dotted line). Besides the evident better agreement obtained by modeling the experimental signal as Cu–O contributions, an F test (46) on both fit results allows one to discard the Cu–Cl model with a confidence level higher than 95%. The adopted statistical test compares only the two extreme cases (100% oxygen vs 100% chlorine scatterers), and intermediate cases cannot be excluded *a priori*. It is however worth noticing that, due to the much higher scattering amplitude of Cl, even a small fraction (about 15–20% as estimated from simulations) of unreacted $CuCl_2$ should originate, in the phase-uncorrected FT, a peak at 1.95 Å emerging from the Cu–O peak at 1.52 Å (see dotted curve in Fig. 6b where the corresponding FT of hydrated $CuCl_2$ is reported). In this regard it is worth recalling that the local structure around the copper ion in hydrated $CuCl_2$ is a highly elongated octahedron (47) showing two short planar distances (two oxygens at 1.95 Å and two chlorines at 2.29 Å, responsible for the two described peaks in the FT of the EXAFS data) and one long axial distance (two oxygens at about 4 Å). The absence of any relevant amount of Cl in the first shell of copper is definitely demonstrated by the application of the Lee and Beni criterion which indicates that when the shell contribution arises from a single atomic type of scatterer, the imaginary part of the phase-corrected and energy-shifted FT must be symmetric with respect to the modulus of the FT (48). This is precisely what occurs by using the Cu–O phase, as shown in Fig. 6c. As expected, a large asymmetry is found by performing the phase correction with the Cu–Cl phase, as reported in Fig. 6d. We can so conclude the EXAFS analysis of low loaded samples by stating that Cu(II) cations are coordinated (within experimental errors) to five oxygen atoms at about 1.92 Å, and that the presence of the Cu–Cl contribution is below the detection capabilities of the technique (about 10% as estimated by simulations). The quality of the EXAFS data collected on the Cu0.5 sample was too poor to allow a safe data analysis; consequently, no attempt was done to measure Cu0.25. In conclusion, the above-discussed results give definitive proof that in the low-concentration samples copper is present as a surface aluminate species formed as a consequence of the occupancy from the Cu(II) cations of some octahedral vacancies of the alumina surface, where a coordination sphere formed by five oxygen atoms is expected. In this regard, our EXAFS results are in fair agreement with those reported by Friedman *et al.* on a 6.1 Cu wt% loaded catalyst obtained from nitrate (42). Samples with higher loadings (8.9 and 16%) clearly show a second shell Cu–Cu contribution typical of the CuO phase, also detected by XRD.

As far as the dispersion of copper in the surface aluminate is concerned, it is a matter of fact that, only at very low copper concentrations, metal ions can be considered as isolated. This fact has been inferred for samples prepared by nitrate on the basis of EPR studies (33, 34, 38, 49–51). When the Cu concentration is increased, the ions can progressively occupy octahedral vacancies. Under these circumstances the Cu(II) ions cannot be considered as isolated. It is however worth noticing that the concept of "isolated species" is technique-dependent. For a technique with a very local character like EXAFS, copper species in sample Cu1.4 are considered as isolated since no significant Cu–Cu contribution has been found above the noise level (Fig. 6b). With the signal-to-noise ratio of our EXAFS data (Fig. 6a, upper curve), we are probably not able to appreciate Cu–Cu distances higher than about 4 Å: note that also the static disorder plays a negative role. On the contrary, EPR feels a small, but still significant, contribution due to spin–spin interaction of two adjacent paramagnetic species (probably two Cu(II) ions), even on sample Cu0.035. The progressive building up of lateral interactions in spinel-like patches could also explain the shift of the CT bands from 43,000 cm^{-1} (Cu0.25 sample) to 40,000 cm^{-1} (Cu1.4. sample) (see Fig. 1).

In conclusion, all the above results definitively prove that in the low loaded samples Cu(II) occupies octahedral vacancies of the alumina surface with the formation of a diluted surface aluminate and that the chlorine anions released upon dissociation of the $CuCl_2$ molecules are not contributing to the first coordination shell of Cu(II). A plausible scheme of the reaction between $CuCl_2$ and the hydroxylated alumina surface is

$$\begin{aligned} &2(>\text{Al–OH}) + CuCl_2 + 2(>\text{Al–OH}) \\ &\quad \rightarrow (>\text{Al–O})_2\text{Cu} + 2HCl + 2(>\text{Al–OH}) \\ &\quad \rightarrow (>\text{Al–O})_2\text{Cu} + 2(>\text{Al–Cl}) + 2H_2O. \end{aligned} \qquad [2]$$

The presence of a surface aluminate requires the formation of Cu–O–Al bonds with the elimination of chlorine. According to Eq. [2], the Cl released from $CuCl_2$ is kept by alumina. This fact is supported by elemental analysis, indicating that the Cl/Cu atomic ratio is constant along the whole set of samples and close to 2 (Fig. 7). Of course, the reaction of $CuCl_2$ with alumina should also induce the formation of >Al–Cl bonds because HCl is reacting with the surface. Kitökivi *et al.* (52), in a well-documented NMR and IR study on the interaction of HCl with bare alumina, found that two reactions can take place, i.e.,

$$>\text{Al–O–Al}< + HCl \rightarrow >\text{Al–OH} + \text{Cl–Al}<, \qquad [3]$$

$$>\text{Al–OH} + HCl \rightarrow >\text{Al–Cl} + H_2O. \qquad [4]$$

The chlorination temperature and the hydroxylation state

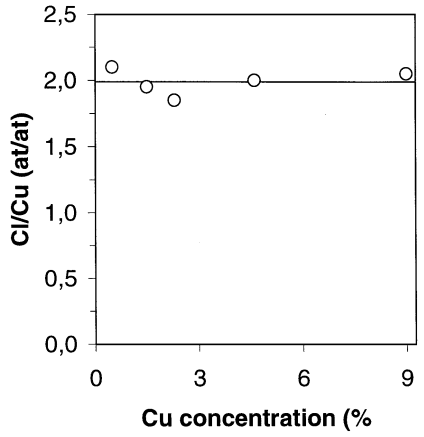

FIG. 7. Cl/Cu atomic ratio vs Cu concentration.

of the alumina are the main factors driving the prevalence of one mechanism against the other, being the second reaction prevalent at short time. In the field of our interest, (i.e., high hydroxylation degree, low temperature, and $CuCl_2$ as the source) the interaction should follow the second mechanism. The amount of chlorine fixed by alumina depends on the temperature and it is about 3 Cl atoms nm^{-2} at 373 K (52). The value is substantially similar to that reported by Bailey and Wightman at 313 K (53) and by Tanaka and Ogosawara at 298 K (54).

The data extracted from the solubility test (Fig. 3) indicate that the maximum achievable concentration of surface aluminate is 1.6 wt% Cu, corresponding to 0.95 wt% Cu/100 m^2 and to 1.06 wt% Cl/100 m^2 (Eq. [2] and Fig. 7). These values represent the maximum capacity of the alumina surface to accommodate Cu and Cl ions derived from copper chloride complexes or, in other words, its saturation point. It is worth noticing that the amount of incorporated chlorine in our samples is lower than that reported when only Cl is hosted (45–47) (1.06 against 1.7 wt% Cl/100 m^2). The same holds for the amount of incorporated copper ions if compared to the same value obtained for samples prepared from nitrate, which is ranging from 3.0 to 5.5 wt% Cu/100 m^2 (34, 38, 55, 56). This fact can be explained on the basis of mechanism [2] because, in our case, available surface sites are shared between Cu cations and Cl anions. Of course, also the considerably different temperature at which the interaction takes place (RT for $CuCl_2/Al_2O_3$ system and more than 570 K for the $Cu(NO_3)_2/Al_2O_3$ one) must play a relevant role since it directly influences the concentration of the OH groups of the alumina surface. However, the number of ions per unit surface corresponding to the maximum coverage is similar in all cases: 2.7 ions nm^{-2} for our samples (hosting both Cu^{2+}, Cl^-); 2.9 anions nm^{-2} for chlorinated alumina (hosting only Cl^-); and 2.8–5.2 cations nm^{-2} for alumina impregnated with copper nitrate (hosting only Cu^{2+}). From this comparison we can conclude that the number of ions hosted on γ-Al_2O_3 surfaces is rather constant, which in turns implies that the maximum number of Cu(II) cations accommodated on the surface in the $CuCl_2/Al_2O_3$ system is limited by the necessity to host Cl^- anions too.

Among the most stable faces of γ-Al_2O_3, the (110) one is a good candidate to be the support surface for Cu(II) cations in the $CuCl_2/Al_2O_3$ system. In fact, the (110) face is largely dominant in alumina with spinel structure (57); moreover, its number of surface octahedral sites (OS) (6.5 nm^{-2}, corresponding to 6.9 wt% Cu/100 m^2) is well compatible with the experimental values reported above. Figure 8 represents the surface aluminate formed on the (110) face of γ-Al_2O_3. In this regard, it is worth noticing that OS lies on parallel rows: the distance between two adjacent OS, bridging one oxygen atom, is $R_{\parallel} = 2.86$ Å while the smallest distances between OS in two adjacent rows is much greater $R_{\perp 1} = 5.72$ Å and $R_{\perp 2} = 6.39$ Å. EXAFS results, not showing significant Cu–O–Cu contributions (at about $R = 2.86$ Å), strongly suggest that the formation of copper spinel phases where the octahedral vacancies are sharing corner or edges is not significant. On the contrary, the alternated presence of two Cu ions on the same row cannot be excluded from EXAFS, since $2R_{\parallel} = 5.72$ Å will be above the sensitivity of the experimental data. The same holds for the simultaneous presence of two Cu(II) ions in the closest sites of two parallel rods ($R_{\perp 1} = 5.72$ Å and $R_{\perp 2} = 6.39$ Å). This hypothesis can explain the origin of the spin–spin interaction detected by EPR, even for sample Cu0.035.

3.3. The Nature of Cu(II) Species on Highly Concentrated Samples

As previously done for the Cu(II) species prevailing at low Cu concentration, we can now briefly summarize the properties of the species dominating on high loaded (freshly prepared) samples: (i) the species is soluble; (ii) it starts to appear when the maximum capacity of the alumina surface to react with $CuCl_2$ is completed (about 1.6 wt% in our set of samples); (iii) it is characterized by a very intense *d–d* band at about 13,000 cm^{-1} and an additional CT band in the 28,000- to 31,000-cm^{-1} range; (iv) it is not stable upon both thermal and vacuum treatments; (v) it shows a very broad EPR signal with spherical symmetry.

XRD gives no useful information for the identification of the structure of such species since the XRD patterns of all samples are identical to that of bare alumina, with the only exception of the Cu9.0 sample (where very weak peaks attributable to paratacamite have been found). This implies that the species present at high concentration must be in an amorphous state, or in the form of nanoclusters having a size falling in the undetectable region of the diffraction technique (less than about 20–30 Å). Although no $CuCl_2$ XRD peaks have been detected, even at highest Cu concentrations, we believe that $CuCl_2$ is the species prevailing

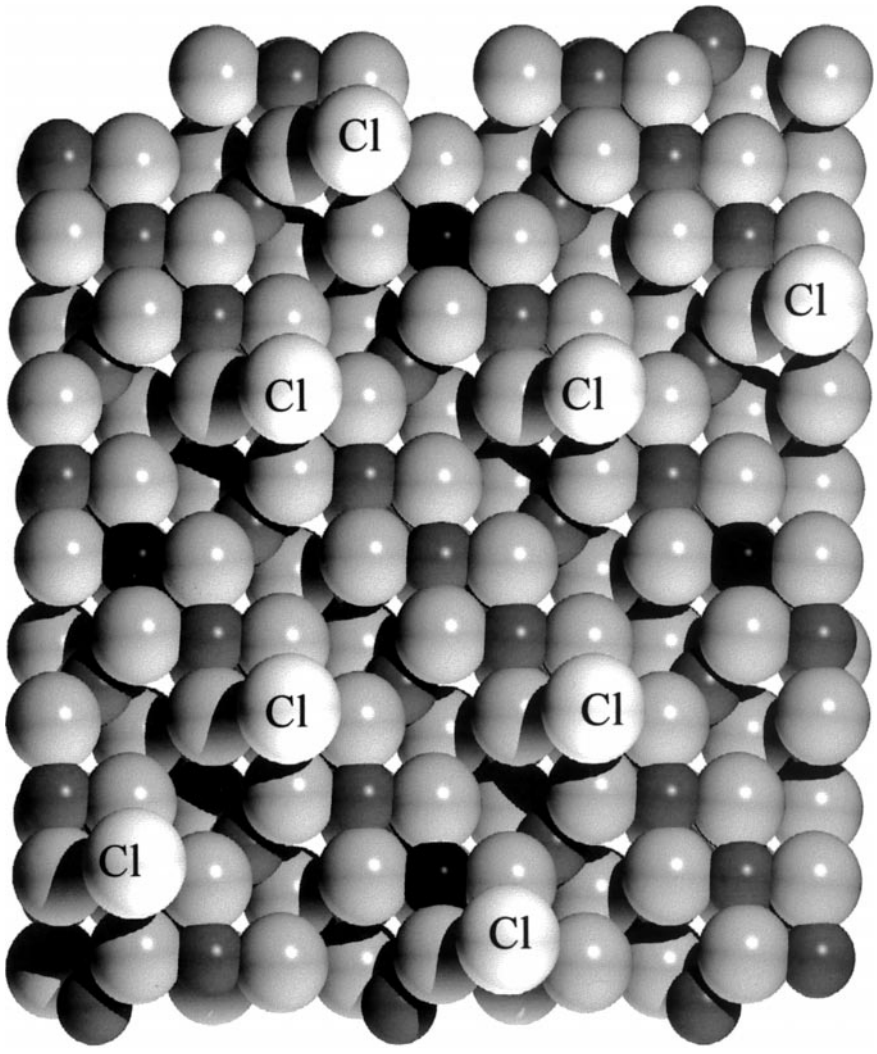

FIG. 8. Al_2O_3 spinel (110) plane, cut at octahedral sites level. Dark and light gray spheres represent aluminum and oxygen atoms, respectively. In some octahedral vacancies Cu(II) cations (black spheres) are placed to obtain a surface distribution in agreement with experimental results. White spheres, labeled with "Cl" and placed on the top of Al^{3+} cations, represent chlorine anions satisfying the Cl/Cu ratio of 2.

at high copper concentration, together with minor amounts of paratacamite.

The first argument in favor of this hypothesis is the presence, at high loading, of a consistent fraction of soluble Cu. As pointed out in the Introduction section, $CuCl_2$ is the only Cu compound, among chlorides, oxychlorides, hydroxychlorides, and oxides, having an appreciable solubility. Moreover, the soluble fraction increases linearly with Cu concentration (Fig. 3): this is the expected behavior if, after completion of the surface aluminate following reaction [2], the excess $CuCl_2$ precipitates from solution inside the pores during the drying process, without interaction with the support surface.

Further proof of the presence of $CuCl_2 \cdot 2H_2O$ is given by the abrupt change in intensity of the *d–d* transition band observed at copper loading ~2.3 wt% and by comparison with the spectrum of unsupported $CuCl_2 \cdot 2H_2O$ (Fig. 1): note that the high intensity of the *d–d* band of $CuCl_2 \cdot 2H_2O$ is due to the presence of two chemically different ligands (Cl and O) in the coordination sphere of Cu(II). In fact, the spectra of the Cu9.0 sample and of hydrated $CuCl_2$ are very similar in the whole range (Fig. 1), although the former is less resolved, probably because of the disorder induced by the support. The same comparison does not hold with paratacamite (see the bottom spectrum in Fig. 2 of Ref. (22)), exhibiting a CT band of different figure and a *d–d* band of intermediate intensity (more than 1 order of magnitude higher than that of the surface alluminate, but 4–10 times lower than $CuCl_2 \cdot 2H_2O$; the actual magnitude of the bands of hydrated $CuCl_2$ cannot be safely evaluated due to the high Kubelka–Munk values). In this regard, it is worth noticing that $Cu_2(OH)_3Cl$ has two equipopulated copper sites, the former being a regular octahedron with six oxygen ligands at 2.11 Å and the latter being an elongated

octahedron with four planar oxygen ligands at 1.98 Å and two axial chlorine ligands at 2.78 Å (58). The still strong intensity of the *d–d* band of paratacamite can be attributed only to Cu(II) in the second site, due to its chemical heterogeneity in the ligand sphere. The effect of the insertion of the chlorine atoms in the coordination sphere of Cu(II) on the *d–d* band intensity is however supposed to be weaker in paratacamite than in hydrated copper chloride due to the higher Cu–Cl distance (2.78 vs 2.29 Å).

The Cu9.0 sample represents the final stage of a spectral evolution starting with the Cu2.3 sample, and associated with the development of a second band in the 28,000- to 31,000-cm^{-1} range, progressively overlapping the band in the 40,000- to 43,000-cm^{-1} range present in the low copper-concentration samples. The consistent difference (about 9,000–11,000 cm^{-1}) between the CT of the two species (surface aluminate and supported $CuCl_2 \cdot 2H_2O$) clearly indicates that a partial substitution of oxygen ligands occurs by passing from low to high concentration species. EXAFS analysis has demonstrated that oxygen is the only copper ligand in the low-concentration species while, according to our hypothesis, the chlorine ligand also is present in the Cu coordination sphere of the high-concentration species. This picture is in fair quantitative agreement with the empirical equation (30)

$$E(\mathrm{CT}) = 30{,}000[\chi_{\mathrm{opt}}(\mathrm{ligand}) - \chi_{\mathrm{opt}}(\mathrm{metal})] \qquad [5]$$

(30,000 being a phenomenological constant given in cm^{-1}). In fact, the difference in optical electronegativity between chlorine ($\chi_{\mathrm{opt}} = 3.0$) and alternative ligands (O^-, $\chi_{\mathrm{opt}} = 3.2$–3.3; OH^-, $\chi_{\mathrm{opt}} = 3.5$; H_2O, $\chi_{\mathrm{opt}} = 3.5$) gives a difference between the corresponding CT band maxima of 6,000–15,000 cm^{-1}.

As already briefly mentioned in the discussion of the EPR data reported in Fig. 4, the evacuation at RT up to 10^{-3} Torr induces, in samples Cu2.3, Cu4.6, and Cu9.0, a color change from green to brown. This experimental evidence, already pointed out in the EPR study by Blanco *et al.* (5), means that the dehydration process does not concern the physisorbed water only, always present in the as-prepared samples, but is also involving the crystallization water of $CuCl_2 \cdot 2H_2O$ (green-colored) yielding to the formation of anhydrous $CuCl_2$, which is a brown compound. In fact, the CT edge observed in the UV–vis spectra of high loaded samples and of $CuCl_2 \cdot 2H_2O$ (Fig. 1) undergoes a consistent red shift during the dehydration process, resulting in about 18,000 cm^{-1} at the final stage (spectra not reported for brevity). In this regard, note that the local structure of anhydrous $CuCl_2$ consists of an elongated octahedron (4 equiv of chlorine atoms at 2.26 Å and 2 axial ones at 2.96 Å (59)). Figure 9a reports the 77 K EPR spectra of Cu9.0 and $CuCl_2$, both in anhydrous conditions. Several attempts have also been done to measure the EPR signal of the Cu9.0 sample after evacuation of physisorbed H_2O

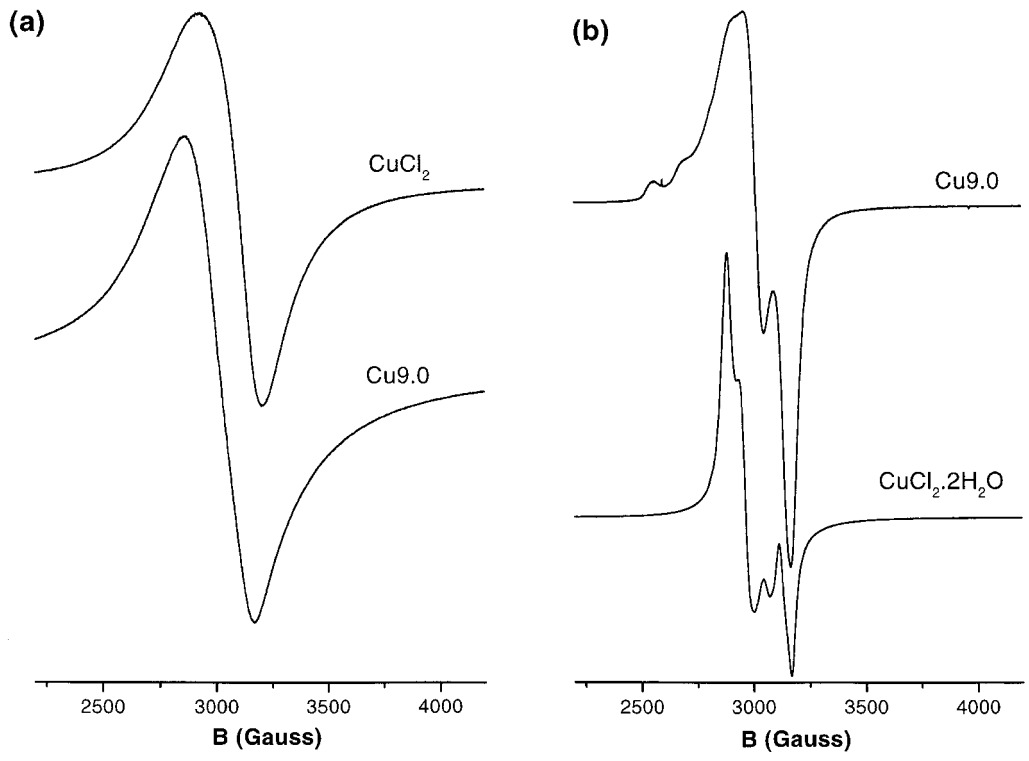

FIG. 9. EPR spectra of $CuCl_2$ and Cu9.0 samples under dehydrated and hydrated conditions: parts (a) and (b), respectively. In part (b) the inversion of the intensities of the $g_\parallel$ and $g_\perp$ components is not a concern.

but without the destruction of the crystallization water of $CuCl_2 \cdot 2H_2O$: this experiment is rather critical due to the instability of the $CuCl_2 \cdot 2H_2O$ nanocrystals upon lowering the pressure. Figure 9b reports the liquid nitrogen temperature EPR spectra of hydrated Cu9.0 and of $CuCl_2 \cdot 2H_2O$. The consistent lost of hyperfine resolution, by moving from the EPR spectrum of the model compound to that of the Cu9.0 sample (Fig. 9b), is probably reflecting the absence of long-range ordering for the Cu(II) species present on the catalyst. The similarities between the EPR spectra collected on the Cu9.0 sample and on copper chloride in both anhydrous and hydrated conditions is further evidence supporting our picture, indicating that the Cu(II) species dominating in high-loaded samples is $CuCl_2 \cdot 2H_2O$ in a highly dispersed amorphous state.

For the sake of completeness, it is worth recalling that the paratacamite traces, found by XRD on the Cu9.0 samples, are the products of a slow hydrolysis of $CuCl_2$ catalyzed by basic sites of the alumina surface. This statement anticipates the results that will be described in the study of the effects of aging (next paper (22)). For the purposes of this work, it is sufficient to emphasize that the presence of this hydroxochloride becomes relevant only on aged samples, and that on fresh samples this slow process is still in a very early stage and can be considered as negligible.

4. CONCLUSIONS

The characterization presented here of copper chloride supported on γ-alumina allows one to obtain a clear picture of freshly impregnated solid. For copper contents lower than 0.95 wt% Cu/100 m^2 of support, the formation of a surface aluminate species takes place: copper occupies octahedral vacancies of the alumina surface and is surrounded (within experimental error) by five oxygen ligands at about 1.92 Å. The metal ions of the surface aluminate are isolated. The chlorine released by $CuCl_2$ during its interaction with alumina reacts with the support, giving $>$Al–Cl species. After completion of the surface alumina adsorptive capacity, copper chloride precipitates directly from the solution during the drying, with the formation of amorphous $CuCl_2 \cdot 2H_2O$, on top of the surface aluminate. A contemporary slow hydrolysis reaction gives traces of insoluble copper hydroxochloride (paratacamite). A dehydration process at RT, up to 10^{-3} Torr, implies the evolution of $CuCl_2 \cdot 2H_2O$, into anhydrous $CuCl_2$ as a consequence of the loss of the crystallization water.

ACKNOWLEDGMENTS

We are strongly indebted to G. L. Marra (EniChem, Istituto G. Donegani), for XRPD measurements, to G. Vlaic (Sincrotrone Trieste and Dipartimento di Chimica Università di Trieste), F. Geobaldo (Politecnico di Torino), and F. Villain (LURE), for their relevant and friendly support during EXAFS measurements, to E. Giamello (Dipartimento di Chimica IFM Università di Torino) for his enlightening contribution in the discussion of the EPR data, and to B. Cremaschi (EVC, Porto Marghera) for her analytical support.

REFERENCES

1. Garilli, M., Fatutto, P. L., and Piga, F., *Chim. Ind.* **80**, 333 (1998).
2. (a) McPherson, R. W., Starks, C. M., and Fryar, G. J., *Hydrocarbon Process.* 75 (1979); (b) Naworski, J. S., and Evil, E. S., *Appl. Ind. Catal.* **1**, 239 (1983).
3. Mross, W. D., *Catal. Rev.-Sci. Eng.* **25**, 591 (1983).
4. (a) Arcoya, A., Cortes, A., and Seoane, X. L., *Can. J. Chem. Eng.* **60**, 55 (1982); (b) Vetrivel, R., Rao, K. V., Seshan, K., Krishnamurthy, K. R., and Prasada Rao, T. S. R., *in* "Proceedings, 9th International Congress on Catalysis, Calgary, 1988" (M. J. Phillips and M. Terran, Eds.), Vol. 5, p. 1766. Chem. Institute of Canada, Ottawa, 1998.
5. Blanco, J., Fayos, J., Garcia De La Banda, J. F., and Soria, J., *J. Catal.* **31**, 257 (1973).
6. Avila, P., Blanco, J., Garcia-Fierro, J. L., Mendioroz, S., and Soria, J. *Stud. Surf. Sci. Catal.* **7B**, 1031 (1981).
7. Baiker, A., Monti, D., and Wokaun, A., *Appl. Catal.* **23**, 425 (1986).
8. Sermon, P. A., Rollins, K., Reyes, P. N., Lawrence, S. A., Martin Luengo, M. A., and Davies, M. J., *J. Chem. Soc., Faraday Trans. 1* **83**, 1347 (1987).
9. Fortini, E. M., Garcia, C. L., and Resasco, D. E., *React. Kinet. Catal. Lett.* **36**, 223 (1988).
10. Garcia, C. L., and Resasco, D. E., *Appl. Catal.* **46**, 251 (1989).
11. Valle, J., Vargas, A., Ferreira, J. M., Flores, A., and Novaro, A., *Stud. Surf. Sci. Catal.* **7B**, 1040 (1981).
12. Zipelli, G., Bart, J. C., Petrini, G., Galvagno, S., and Cimino, C., *Z. Anorg. Allg. Chem.* **502**, 199 (1983).
13. Fortini, E. M., Garcia, C. L., and Resasco, D. E., *J. Catal.* **99**, 12 (1986).
14. Sai Prasad, P. S., and Kanta Rao, P., *J. Chem. Soc., Chem. Commun.* 951 (1987).
15. Rouco, A. J., *Appl. Catal. A* **117**, 139 (1994).
16. Ott, R. J., and Baiker, A., *Stud. Surf. Sci. Catal.* **16**, 685 (1982).
17. Baiker, A., and Holstein, W. L., *J. Catal.* **84**, 178 (1983).
18. Bond, G. C., Namijo, S. N., and Wakeman, J. S., *J. Mol. Catal.* **64**, 305 (1991).
19. Arcoya, A., Cortes, A., and Seoane, X. L., *Can. J. Chem. Eng.* **60**, 55 (1982).
20. (a) Solomonik, I. G., Kurlyandskaya, I. I., Ashavskaya, G. A., and Yakerson, V. I., *Izv. Akad. Nauk. SSSR Ser. Khim.* **4**, 766 (1986); (b) Solomonik, I. G., Kurlyandskaya, I. I., Yakerson, V. I., Kudryavtseva, T. F., Ashavskaya, G. A., Frid, M. R., Treger, Yu. A., and Sonin, E. V., *Izv. Akad. Nauk. SSSR Ser. Khim.* **11**, 2431 (1984).
21. (a) Dotson, R. L., *J. Catal.* **33**, 210 (1974); (b) Sorokin, Yu. M., Bakshi, Yu. M., and Gel'bshtein, A. I., *Kinet. Katal.* **17**, 1023 (1976); (c) Bakshi, Yu. M., Dmitrieva, M. P., and Gel'bshtein, A. I., *Kinet. Katal.* **25**, 136 (1984); (d) Hall, P. G., Heaton, P., and Rosseinsky, D. R., *J. Chem. Soc., Faraday Trans. 1* **80**, 2785 (1984); (e) Solomonik, I. G., Kurlyandskaya, I. I., Danyushevskii, V. Ya., and Yakerson, V. I., *Izv. Akad. Nauk. SSSR Ser. Khim.* **10**, 2175 (1984); (f) Solomonik, I. G., Kurlyandskaya, I. I., Danyushevskii, V. Ya., and Yakerson, V. I., *Izv. Akad. Nauk. SSSR Ser. Khim.* **10**, 2180 (1984); (g) Dmitrieva, M. P., Bahshi, Yu. M., and Gel'bshtein, A. I., *Kinet. Katal.* **26**, 1359 (1985); (h) Kurlyandskaya, I. I., Dasheveskii, M. I., Solomonik, I. G., Kudryavtseva, T. F., and Yakerson, V. I., *Kinet. Katal.* **6**, 1220 (1987); (i) Garcia, C. L., and Resasco, D. E., *J. Catal.* **122**, 151 (1990).
22. Leofanti, G., Padovan, M., Garilli, M., Carmello, D., Marra, G. L., Zecchina, A., Spoto, G., Bordiga, S., and Lamberti, C., **189**, 105 (2000).
23. Sneed, M. C., Maynard, J. L., and Brasted, R. C., "Comprehensive Inorganic Chemistry," Vol. 2. D. Van Nostrand Company, New York, 1954.

24. (a) Lamberti, C., Bordiga, S., Salvalaggio, M., Spoto, G., Zecchina, A., Geobaldo, F., Vlaic, G., and Bellatreccia, M., *J. Phys. Chem. B* **101**, 344 (1997); (b) Zecchina, A., Bordiga, S., Turnes Palomino, G., Scarano, D., Lamberti, C., and Salvalaggio, M., *J. Phys. Chem. B* **103**, 3833 (1999); (c) Lamberti, C., Bordiga, S., Zecchina, A., Salvalaggio, M., Geobaldo, F., and Otero Areàn, C., *J. Chem. Soc., Faraday Trans.* **94**, 1519 (1998).
25. Michalowicz, A., *J. Phys. IV (France)* **7**, C2–235 (1997).
26. (a) Lytle, F. W., Sayers, D. E., and Stern, E. A., *Physica B* **158**, 701 (1989); (b) Durham, P. J., *in* "X-Ray Absorption" (D. C. Koningsberger and R. Prins, Eds.), p. 53. Wiley & Sons, New York, 1988.
27. McKale, A. G., Veal, B. W., Paulikas, A. P., Chan, S. K., and Knapp, G. S., *J. Am. Chem. Soc.* **110**, 3763 (1988).
28. Restori, R., and Schwarzenbach, D., *Acta Crystallogr. B* **42**, 201 (1986).
29. Asbrink, S., and Waskowska, A., *J. Phys. Condensed Matter* **3**, 8173 (1991).
30. Jorgensen, C. K., *Prog. Inorg. Chem.* **12**, 101 (1979).
31. Giamello, E., Murphy, D., Magnacca, G., Morterra, C., Shioya, Y., Nomura, T., and Anpo, M., *J. Catal.* **136**, 510 (1992).
32. Sharpe, P. K., and Vickerman, S. C., *in* "Proceedings, 6th International Congress on Catalysis, London, 1976" (G. C. Bond, P. B. Wells, and F. C. Tompkins, Eds.), p. A14. The Chemical Society, London, 1976.
33. Berger, P. A., and Rooth, J. F., *J. Phys. Chem.* **71**, 4307 (1967).
34. Zhang, Y,. Zeng, X., and Keng, T., *React. Kinet. Catal. Lett.* **43**, 387 (1991).
35. Lumbeck, H., and Voitländer, J., *J. Catal.* **13**, 117 (1969).
36. Losee, D. B., Kassman, A. J., and Wilson, P. A., *J. Catal.* **67**, 226 (1981).
37. Strohmeier, B. R., Leyden, D. E., Scott Field, R. S., and Hercules, D. M., *J. Catal.* **94**, 514 (1985).
38. Kazanov, N., Vorob'ev, V. N., and Talipov, G. Sh., *Kinet. Katal.* **19**, 730 (1978).
39. Hierl, R., Knözinger, H., and Urbach, H. P., *J. Catal.* **69**, 475 (1981).
40. Marion, M. C., Garbowski, E., and Primet, M., *J. Chem. Soc., Faraday Trans.* **86**, 3027 (1990).
41. Lo Jacono, M., Cimino, A., and Inversi, M., *J. Catal.* **76**, 320 (1982).
42. Friedman, R. M., Freeman, G. J., and Lytle, F. W., *J. Catal.* **55**, 10 (1978).
43. Diez Viñuela, J. S., Otero Arean, C., and Stone, F. S., *J Chem. Soc., Faraday Trans. 1* **79**, 1191 (1983).
44. Centi, G., Perathoner, S., Biglino, D., and Giamello, E., *J. Catal.* **151**, 75 (1995).
45. (a) Prins, R., and Koningsberger, D. C., *in* "X-Ray Absorption" (D. C. Koningsberger and R. Prins, Eds.), p. 321. Willey & Sons, New York, 1988; (b) Bart, J. C., and Vlaic, G., *Adv. Catal.* **35**, 1 (1987).
46. (a) Joyner, R. W., Martin, K. J., and Meehan, P., *J. Phys. C* **20**, 4005 (1987); (b) Freund, J., *Phys. Lett. A* **157**, 256 (1991).
47. Engberg, A., *Acta Chim. Scand.* **24**, 3510 (1970).
48. (a) Lee, P. A., and Beni, G., *Phys. Rev. B* **15**, 2862 (1977); (b) Sayers, D. E., and Bunker, B. A., *in* "X-Ray Absorption" (D. C. Koningsberger and R. Prins, Eds.), p. 221. Wiley, New York, 1988.
49. Voge, H. H., and Atkins, L. T., *J. Catal.* **1**, 171 (1962).
50. Wolberg, A., and Roth, J. F., *J. Catal.* **15**, 250 (1969).
51. Wolberg, A., Ogilvie, J. L., and Roth, J. F., *J. Catal.* **19**, 86 (1970).
52. Kytökivi, A., Lindblad, M., and Root, A., *J. Chem. Soc., Faraday Trans.* **91**, 941 (1995).
53. Bailey, R. R., Wightman, J. P., and Root, A., *J. Colloid Interface Sci.* **70**, 112 (1979).
54. Tanaka, M., and Ogasawara, S., *J. Catal.* **16**, 157 (1970).
55. Jacobson, P. E., and Selwood, P. W., *J. Am. Chem. Soc.* **76**, 2641 (1954).
56. Selwood, P. W., and Dallas, N. S., *J. Am. Chem. Soc.* **70**, 2145 (1948).
57. Marchese, L., Bordiga, S., Coluccia, S., Martra, G., and Zecchina, A., *J. Chem. Soc., Faraday Trans.* **89**, 3483 (1993).
58. Fleet, M. E., *Acta Crystallogr. B* **31**, 183 (1975).
59. Burns, P. G., and Hawthorne, F. C., *Am. Mineral.* **78**, 187 (1993).